

NATIONAL TRANSPORTATION SAFETY BOARD

Office of Research and Engineering
Materials Laboratory Division
Washington, D.C. 20594



November 30, 2015

MATERIALS LABORATORY FACTUAL REPORT

Report No. 15-096

1. ACCIDENT

Place : Lolo Pass, Idaho
Date : July 28, 2014
Vehicle : Lancair Legacy, N29MM
NTSB No. : WPR14FA316
Investigator : Albert Nixon, AS-WPR

2. COMPONENTS EXAMINED

Pieces of #1 Connecting Rod
Pieces of #2 Connecting Rod

3. DETAILS OF THE EXAMINATION

On July 28, 2014, about 0853 Pacific daylight time, an amateur-built experimental Meyer-Lancair Legacy sustained substantial damage during a forced landing following a reported loss of engine power during cruise flight. The commercial pilot, sole occupant of the airplane, was fatally injured. The flight departed Richland Airport (RLD), Richland, Washington, at an undetermined time with a destination of Baker Municipal Airport, Baker, Montana. The wreckage was located by law enforcement personnel in mountainous terrain near Lolo Pass, Idaho.

A Federal Aviation Administration inspector examined the airplane at the accident site. The airplane's fuselage and wings were substantially damaged. All major structural components of the airplane were present in the wreckage debris path. The wreckage was recovered to a secure location for further examination. The #1 and #2 connecting rod assemblies were removed from the Continental IO-550-N36B engine (S/N TC5821) and sent to the NTSB Materials Laboratory.¹

Figure 1 illustrates the two connecting rod assemblies, as received. Both connecting rods had been substantially damaged—both had fractured along the I-beam shafts, with a portion of the #2 connecting rod shaft having bent backward in an approximately 45° angle. Both assemblies exhibited impact batter, consistent with post fracture damage. The #2 rod cap was deformed, and the remaining rod bolt had fractured (the other bolt was missing).

¹ The Continental IO-550 engine is a large family of fuel injected six-cylinder, horizontally opposed, air-cooled aircraft engines that were developed for use in light aircraft by Teledyne Continental Motors. The IO-550-N has 310 hp (231 kW) at 2700 rpm, with a dry weight of 429.97 lb (195.03 kg). It is similar to the IO-550-G but with increased power rating.

The #1 connecting rod was visibly deformed on the yoke side, with one fractured bolt and one bent bolt. One of the #1 rod bearing inserts was present—this component exhibited galling wear, scraping, and chipping consistent with contact with an adjacent crankshaft bearing surface. The markings on this bearing insert read:

05-10 H SA642398 FAA-PMA GVBS VP3N.

3.1 The #1 Connecting Rod Assembly

The fractured #1 connecting rod exhibited serial markings, but the shaft fracture was collocated at this position, masking some of the digits. The remaining visible markings read:

6320416...M ©.

Figure 2 illustrates the fracture surface of the #1 connecting rod shaft from the piston pin end. The majority of the fracture surface had been obliterated by smearing, consistent with post-fracture damage. A portion of the fracture surface (upper left in Figure 2) exhibited features consistent with crack arrest marks.

The mating fracture surface, shown in Figure 3, was also heavily smeared and damaged. A portion of the fracture surface (lower right of Figure 3) exhibited crack arrest marks. This area is magnified in Figure 4 and Figure 5. The morphology of the crack arrest marks were consistent with progressive fracture that initiated at or near the rod shaft surface and progressed inward (arrows in Figure 5). The circular tear in this region in Figure 4 and Figure 5 was consistent with subsequent post-fracture damage.

This portion of the fracture surface was examined in a scanning electron microscope (SEM). Figure 6 and Figure 7 illustrate typical areas in the progressive region of the #1 connecting rod fracture surface. This region exhibited striations consistent with fatigue crack propagation. Examination of the crack initiation site revealed no additional features, due to the extensive post-fracture damage in the region.

The #1 connecting rod was sectioned just below the fracture surface on the crankshaft side. This cross section was mounted, polished, and etched to examine the microstructure. Figure 8 and Figure 9 show one area of note, located just below the fatigue crack initiation site. The majority of the interior rod shaft microstructure exhibited features consistent with tempered martensite.² However, as shown in both figures, the surface of the rod shaft exhibited a tempered martensite microstructure containing more ferrite (lighter phase), and a darker-colored surface layer, consistent with fine untempered martensite and a highly deformed layer.³ The untempered martensite was consistent with local high heating and rapid quenching. These features were consistent with a high friction area, consistent with contact between the connecting rod shaft and the dissimilar material shown

² Martensite is the metastable phase present in steel alloys produced by rapid quenching from temperatures where the high temperature austenite phase is stable. As viewed in a microscope, martensite is acicular in appearance, generally characterized as hard but brittle material, typically requiring tempering to relieve residual stresses and increase ductility.

³ Ferrite is the stable room temperature iron-rich phase present in steels with lower carbon contents. Ferrite is generally characterized as soft due to its low solubility for carbon.

in Figure 9. Away from this area, corrosion pits were also observed on the surface of the shaft cross section, away from the area shown in Figure 8.

Attached to the shaft surface was a separate material, exhibiting a pearlite/ferrite microstructure consistent with many carbon steels.⁴ The microstructure of this material was noticeably different from the shaft material, and was collocated with smeared material present on the shaft rail face in this location. Inspection of the chemical composition of this material using energy dispersive x-ray spectroscopy (EDS) revealed a low-alloy carbon steel composition. Inspection of the shaft cross-section using EDS and x-ray fluorescence (XRF) found it to be consistent with a type 43XX-series alloy steel.

The bolt holes of the #1 connecting rod yoke and the rod cap were examined. Figure 10 illustrates the bolt holes from the #1 rod yoke side (Figure 10b was the location of the fractured bolt). Both surfaces shown in Figure 10 exhibited circumferential wear marks. However, the wear pattern in Figure 10a was more severe, with visible gouging and smearing marks (see Figure 11). Inside the bolt holes, there were no indications of deep wear or excessive contact. The circumferential wear marks inside the bolt holes were consistent with normal service conditions. There were no visible longitudinal wear marks present in the bolt holes.

Figure 12 shows the fracture bolt that was present in the bolt hole in Figure 10a. The bolt had been bent towards the fracture surface, with indications of local necking deformation adjacent the fracture surface. The fracture surface, shown in Figure 13, exhibited a reflective luster with a relatively rough texture. Examination in the SEM revealed dimple rupture, consistent with overstress failure of the bolt (see Figure 14).

3.2 The #2 Connecting Rod Assembly

The fractured #2 connecting rod exhibited serial marking, but the shaft fracture and bend was located at this position, masking most of the digits. The bent portion was sectioned, and the remaining markings read:

...32041F M © G.

The fracture surface of the #2 connecting rod is illustrated in Figure 15. The fracture surface showed indications of heat tinting on the fracture surface. The fracture surface showed small regions with features consistent with progressive failure. Portions of the fracture surface close to the surface exhibited crack arrest marks, consistent with progressive fracture.

Examination of the progressive portions of the fracture surface using SEM revealed faint fatigue striations (see Figure 16). The remainder of the fracture surface exhibited dimple rupture, consistent with overstress failure, as shown in Figure 17. Examination of the surface of the #2 connecting rod shaft in the fatigue regions of the fracture surface

⁴ Pearlite is a lamellar mixture of ferrite and cementite (Fe_3C) phases resulting from slower cooling above the austenite transformation temperature.

revealed multiple crack initiation sites (see Figure 18). These sites were free of any material artifacts such as inclusions, pores, or corrosion pits.

Below the fracture surface on the side of the shaft of the #2 connecting rod were areas of multiple secondary cracks. These cracks were oriented parallel to the fracture surface, as shown in Figure 19. Figure 20 shows a closer view one of these secondary cracks. The features inside the secondary cracks were consistent with fatigue striations propagating inward.

Figure 21 illustrates a cross-section of the #2 connecting rod, parallel to the grain direction (perpendicular to the secondary crack and fracture surface). Two of the smaller secondary cracks were present in this cross section. The microstructure was consistent with tempered martensite, particularly towards the interior. Closer to the surface, the rod microstructure contained more ferrite (lighter colored phase).

The submitted bolt from the #2 assembly had fractured. The bolt exhibited local necking deformation adjacent the fracture surface. Examination of the fracture surface revealed dimple rupture. These features were consistent with tensile overstress failure of the bolt.

3.3 Microindentation Hardness

The mounted and polished cross-sections of the #1 and #2 connecting rod shafts were tested to determine the local material hardness. The hardness was inspected using microindentation per ASTM E384.⁵ The hardness indents were performed from the surface layer towards the interior of both rods. The hardness results for the #1 connecting rod and the #2 connecting rod are displayed in Figure 22 and Figure 23, respectively.

The hardness results indicated that the rod shafts exhibited lower hardness towards the surface. The average hardness towards the interior of the #1 and #2 connecting rod shafts averaged 32 HRC (315 HV₅₀₀) and 30 HRC (303 HV₅₀₀), respectively. This hardness decreased approximately 10% and 25% towards the surface on the #1 and #2 shaft surfaces. The lower hardness measurements were primarily present up to depths of 0.03 inches, which corresponded with the higher ferrite illustrated in Figure 8 and Figure 21. These characteristics were consistent with partial surface decarburization of the connecting rod shafts.⁶

Erik Mueller
Materials Research Engineer

⁵ ASTM E384 – *Standard Test Method for Knoop and Vickers Hardness of Materials*. ASTM International, West Conshohocken, PA

⁶ Decarburization is the loss of carbon from the surface of a carbon-containing alloy (steel) due to a reaction with one or more substances in a medium that contacts the surface (oxygen in air). Decarburization is typically observed in parts processed in improper furnace atmospheres during high temperature manufacturing.



Figure 1 – The #1 and #2 connecting rod assemblies, as received.

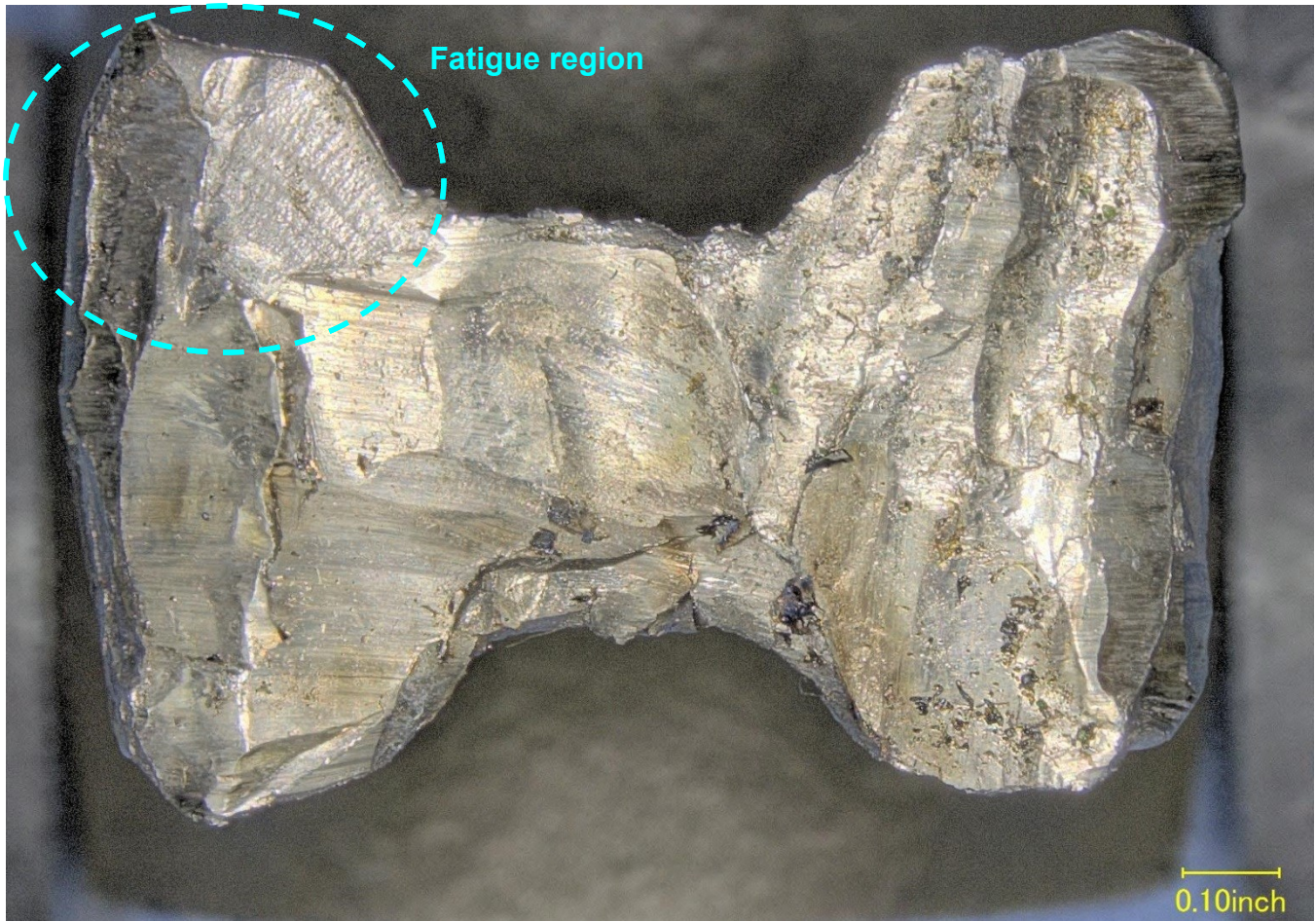


Figure 2 – The fracture surface of the #1 connecting rod in the shank, from the piston pin end.

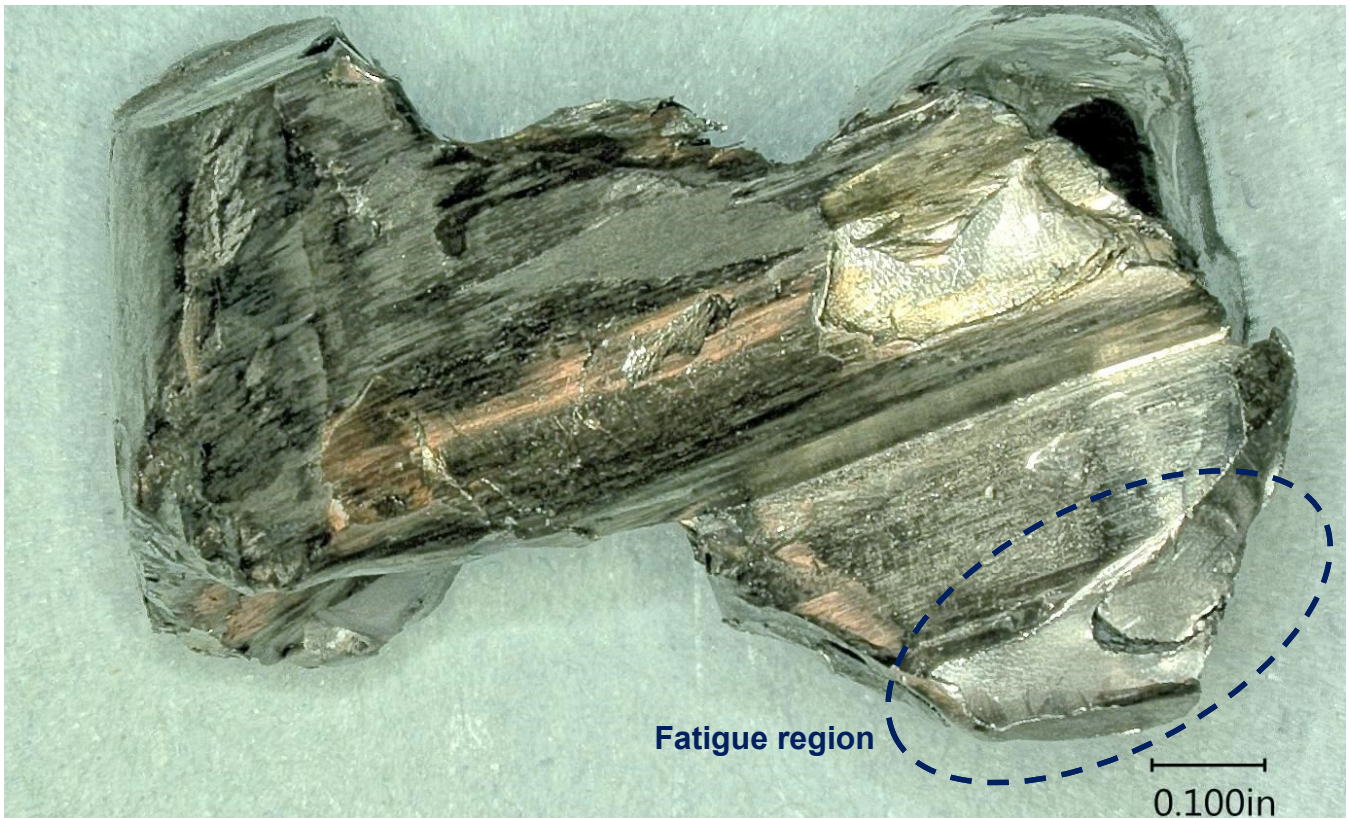


Figure 3 - The fracture surface of the #1 connecting rod in the shank, from the crank end. The area in the lower right is magnified in Figure 4.

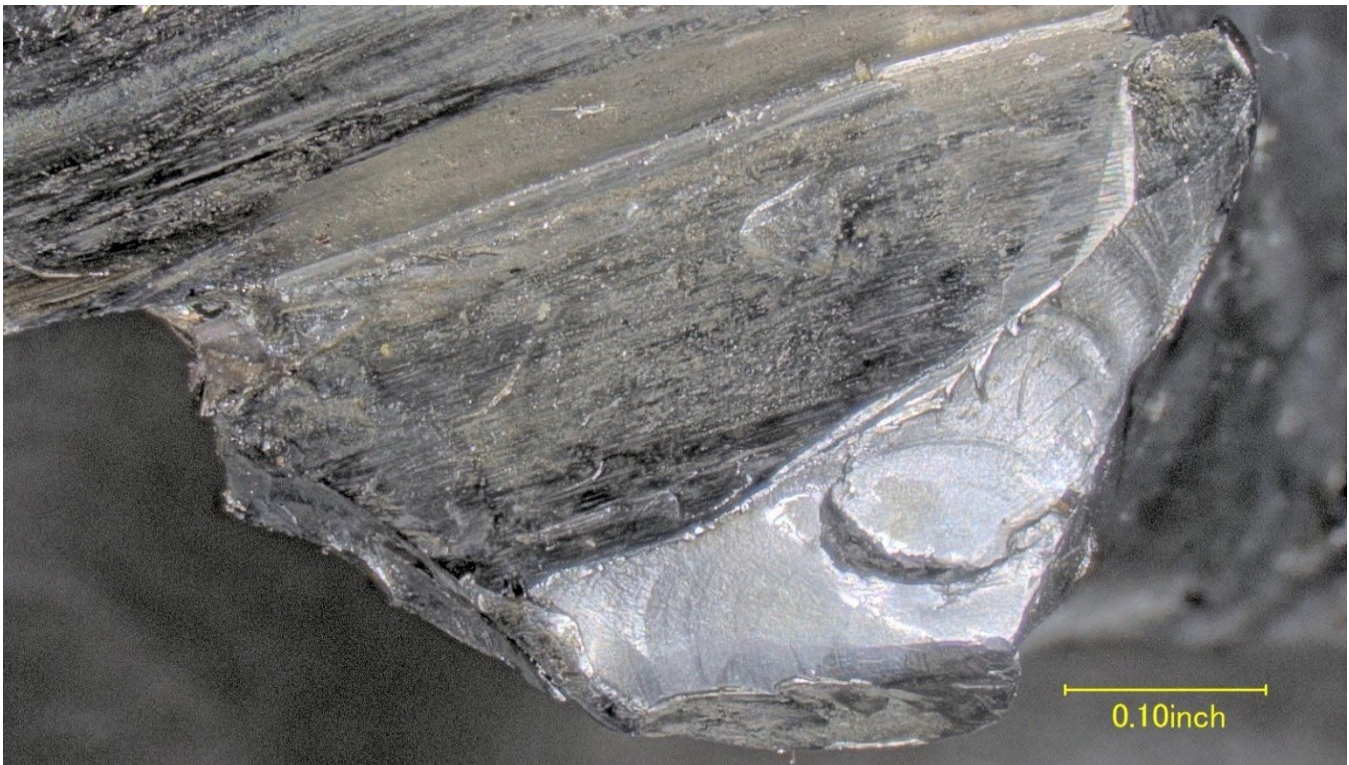


Figure 4 – Closer view of the #1 rod fracture surface from the crank end, showing crack arrest marks (lower right).

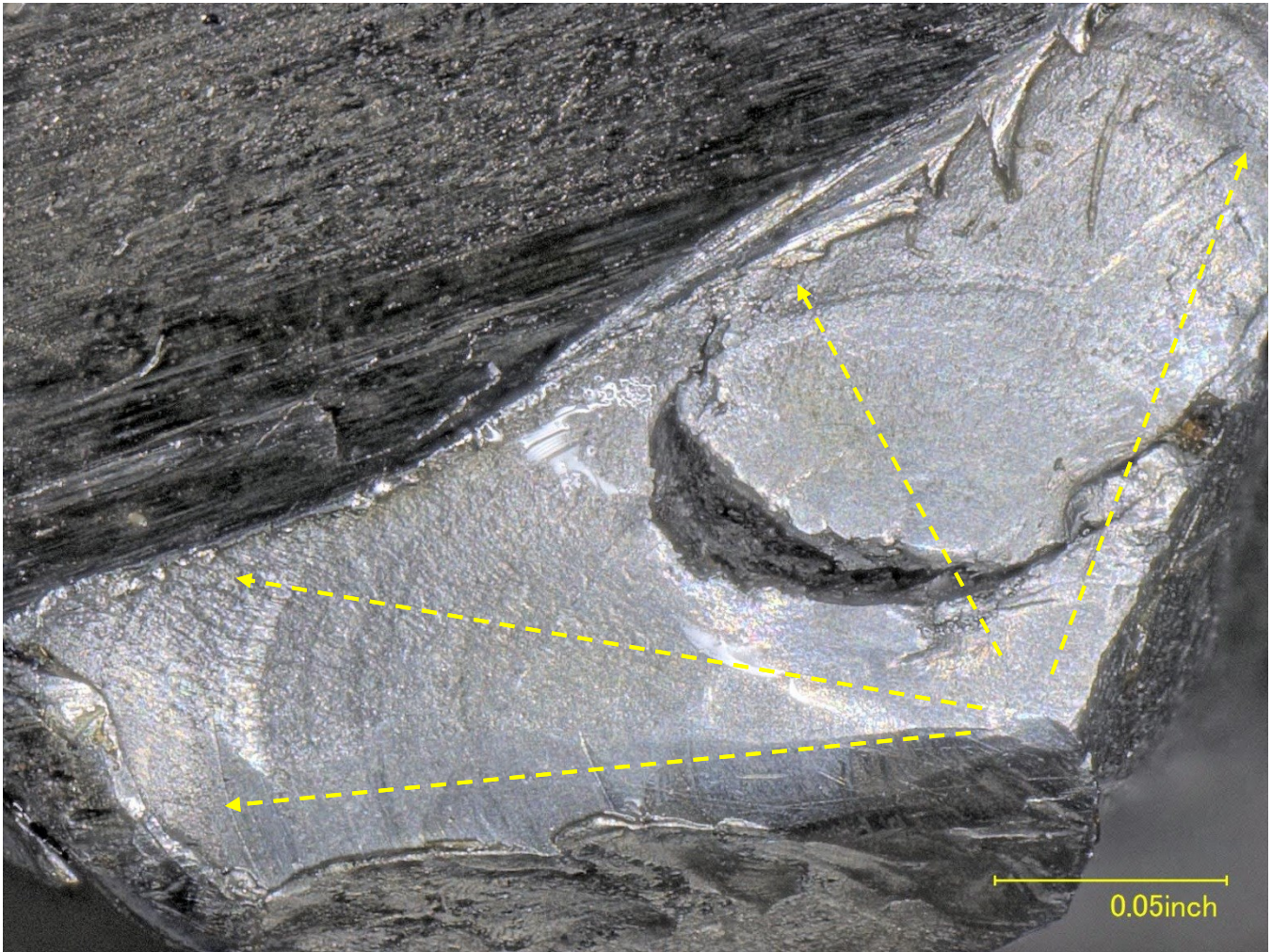
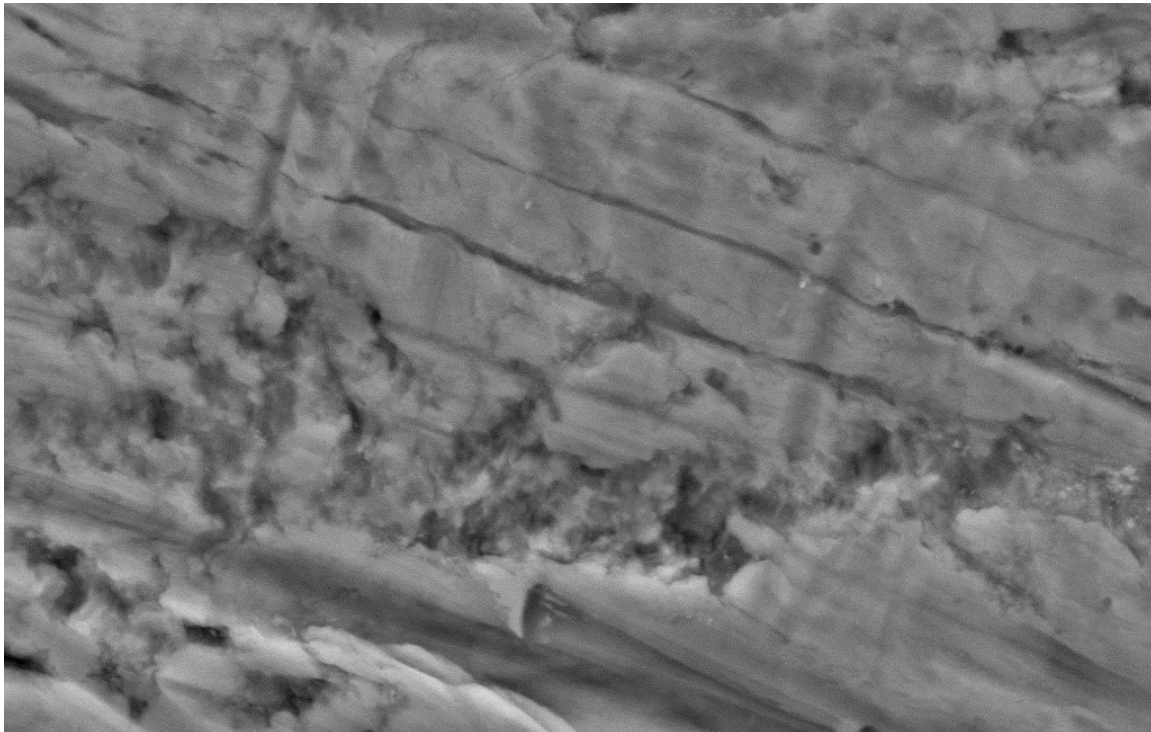


Figure 5 – Closer view of the progressive fracture from the #1 connecting rod shown in Figure 4.



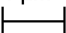
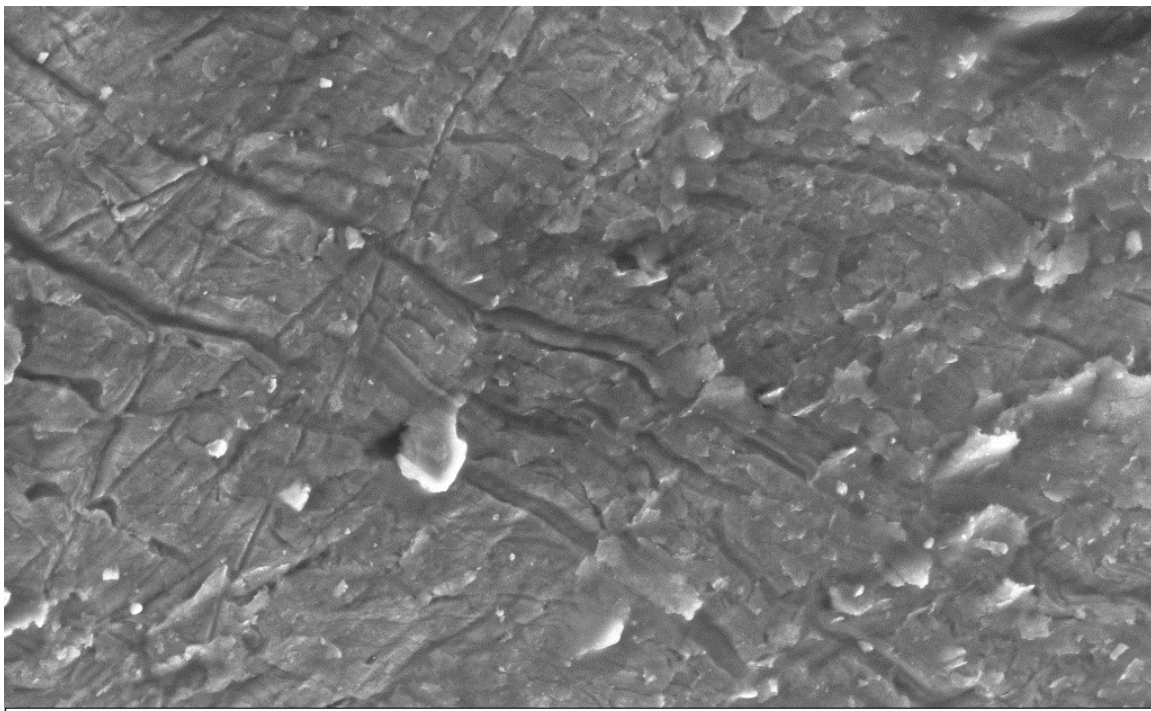
1 μm	EHT = 20.00 kV	Mag = 16.29 K X	Signal A = NTS BSD	NTSB Materials Lab
	WD = 7.4 mm	Width = 18.47 μm	Aperture Size = 30.00 μm	Date :8 Sep 2015

Figure 6 – Backscattered electron (BE) micrograph of fatigue striations in the progressive fracture region of the #1 connecting rod fracture surface from Figure 5.



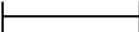
10 μm	EHT = 20.00 kV	Mag = 3.59 K X	Signal A = InLens	NTSB Materials Lab
	WD = 11.9 mm	Width = 83.83 μm	Aperture Size = 30.00 μm	Date :8 Sep 2015

Figure 7 – Secondary electron (SE) micrograph of fatigue striations on the #1 connecting rod fracture surface.

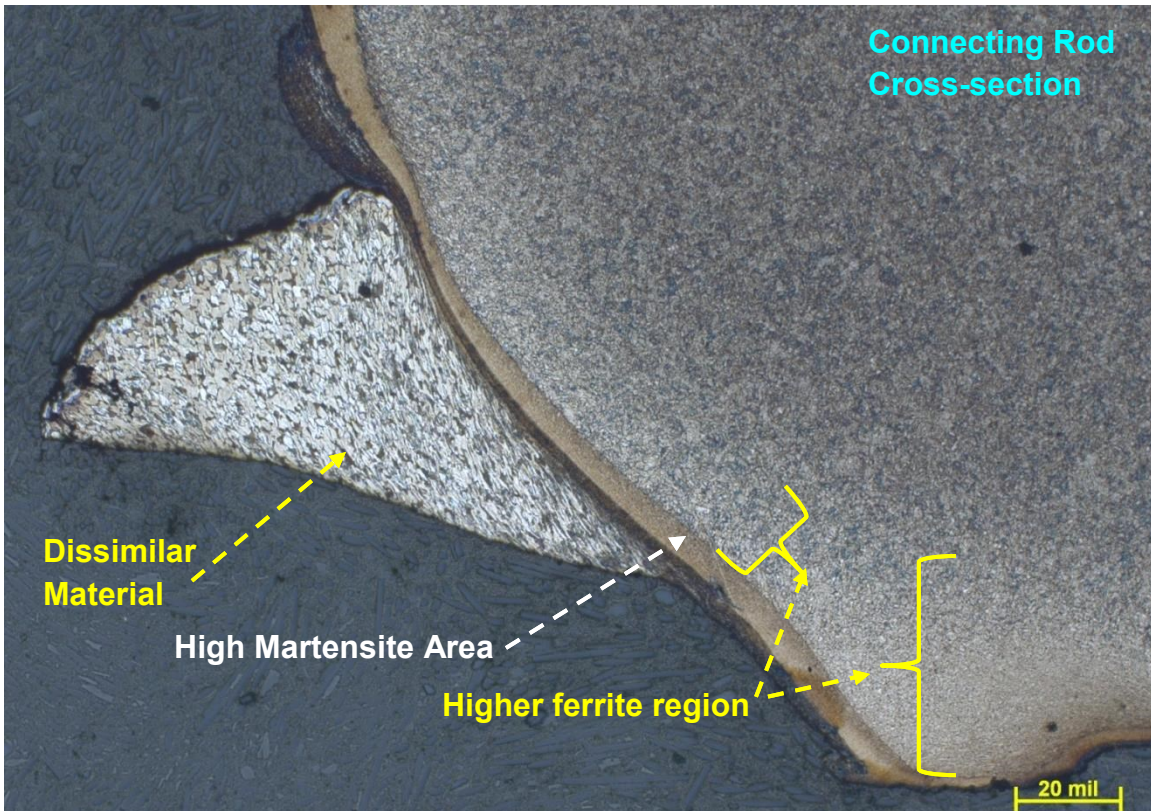


Figure 8 – Optical metallograph of a corner of the #1 connecting rod shaft cross-section, showing deposited foreign material joined to the rod (etched 2% Nital).

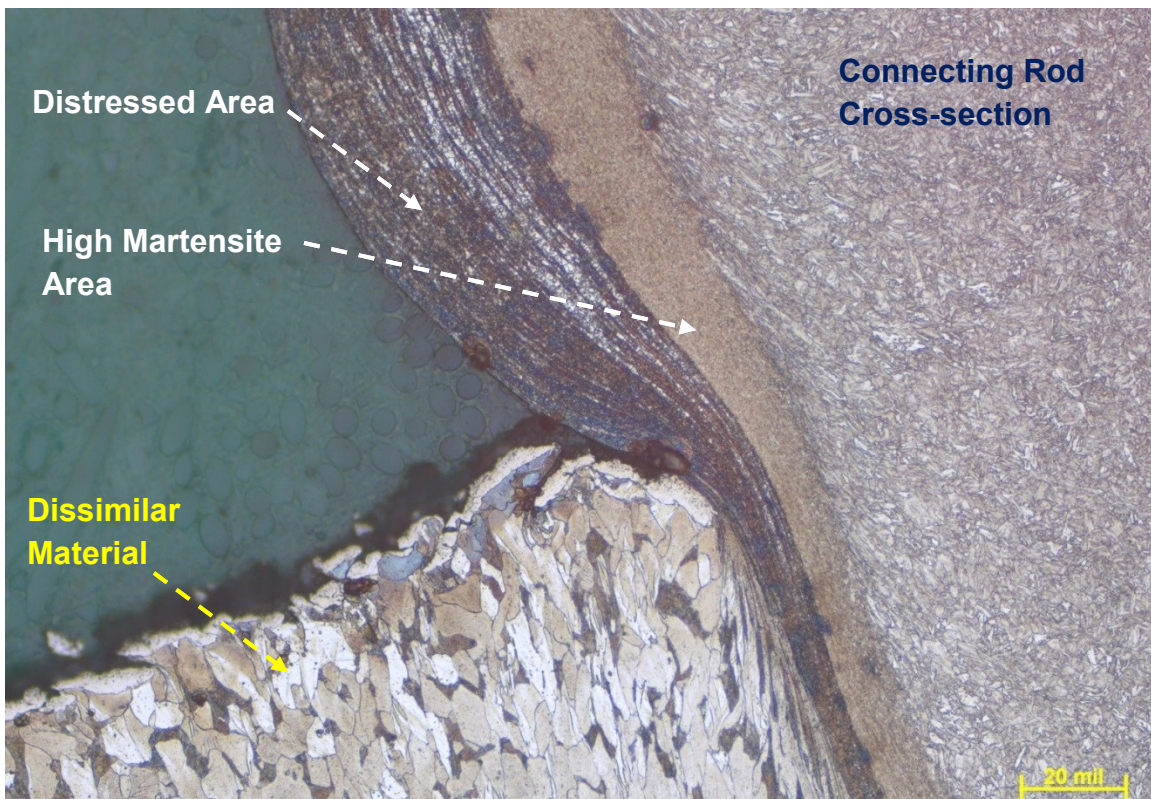


Figure 9 – Closer view of Figure 8, showing the foreign material, attached to the distressed surface layers of the #1 connecting rod (etched 2% Nital).

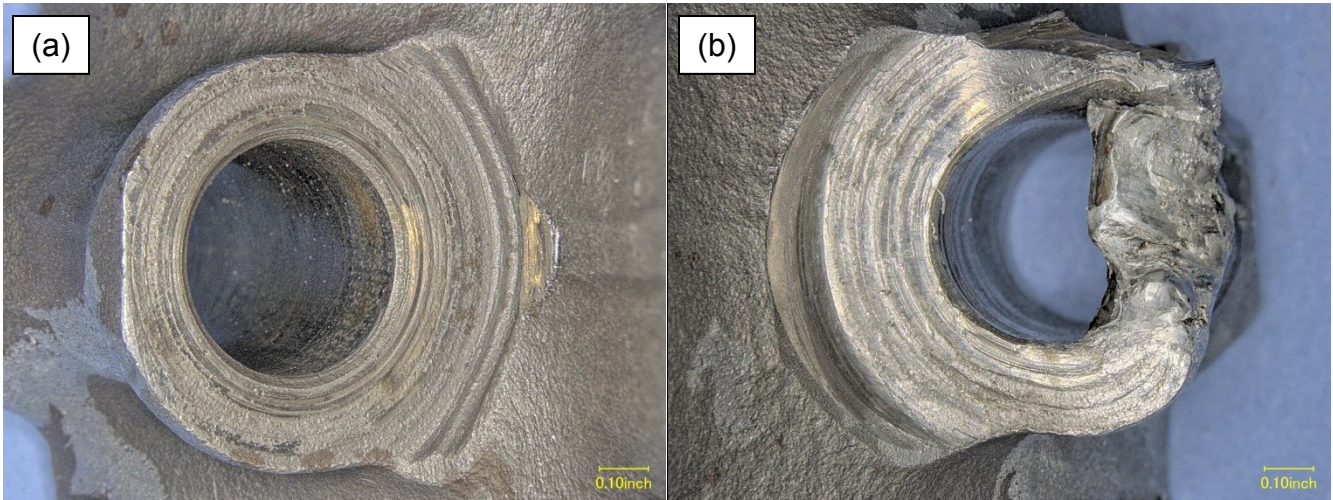


Figure 10 – The bolt holes from the #1 connecting rod yoke.

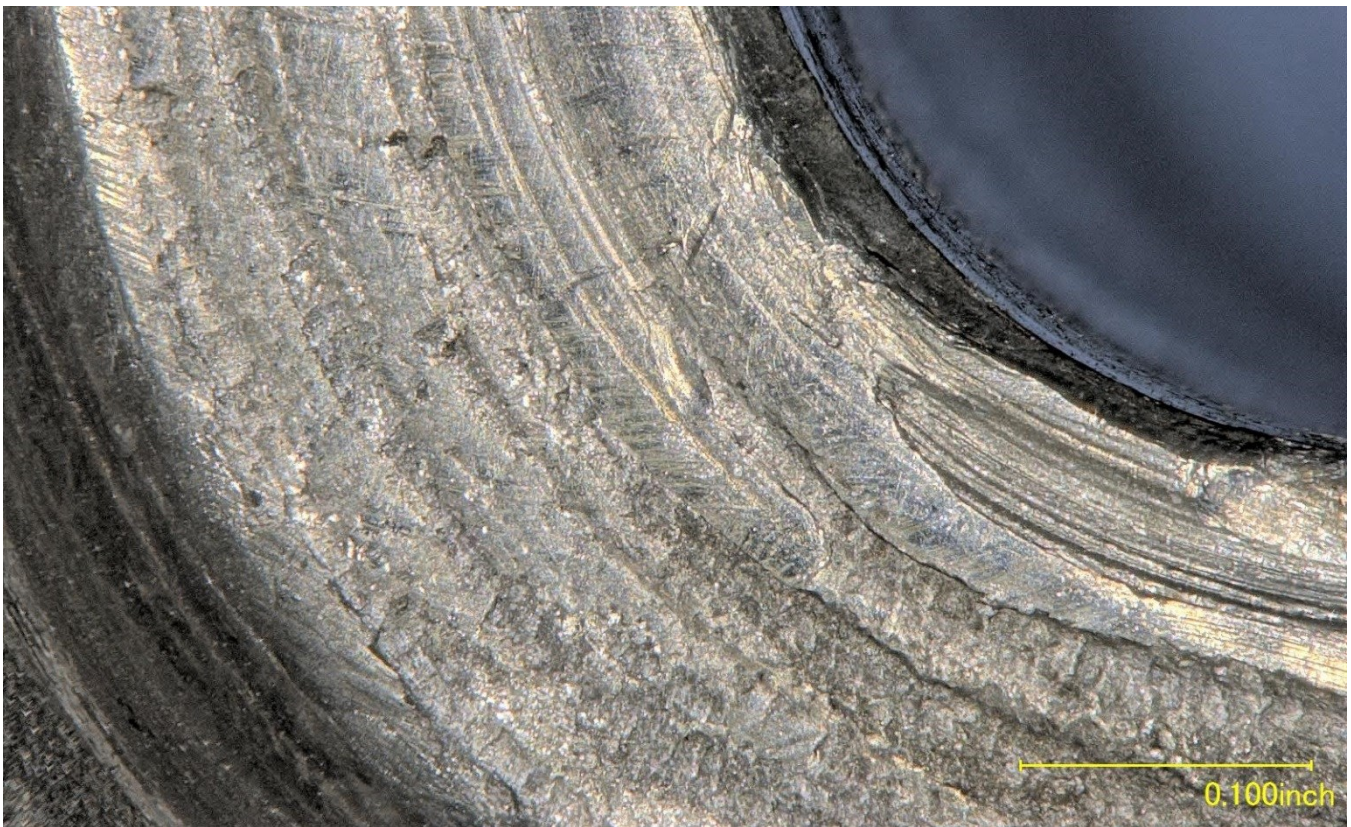


Figure 11 – Closer view of Figure 10a, showing gouging and smearing on the rod surface.



Figure 12 – The #1 connecting rod yoke bolt (positioned on the right in Figure 1), as viewed from the side.

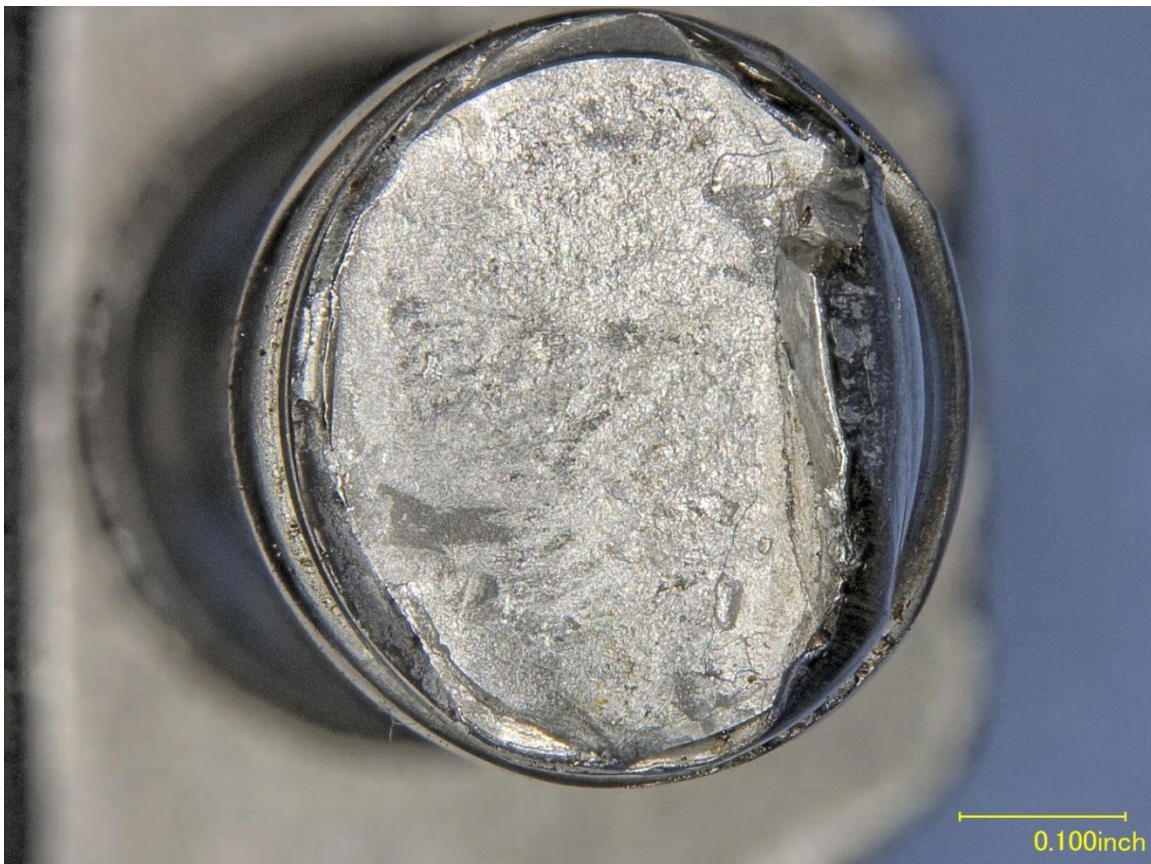


Figure 13 – The fracture surface of the #1 rod yoke bolt, shown in Figure 12.

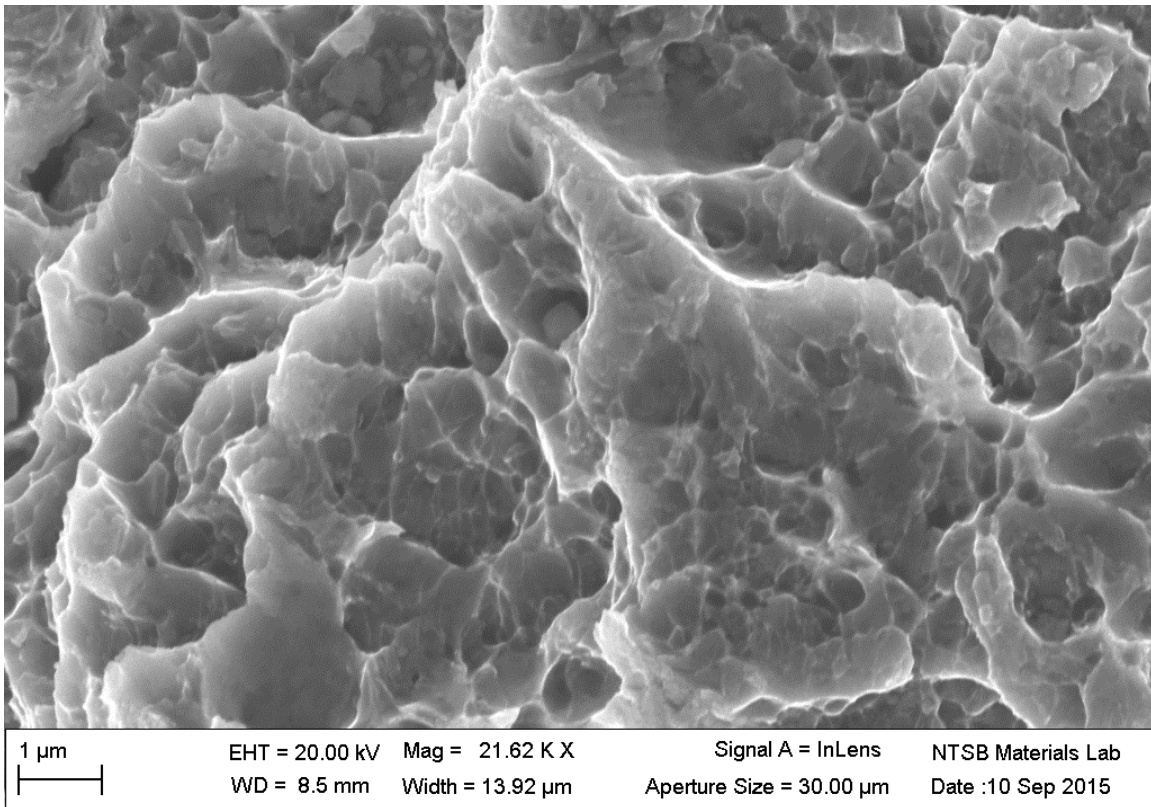


Figure 14 – SE micrograph of the #1 bolt fracture surface, showing dimple rupture consistent with overstress.

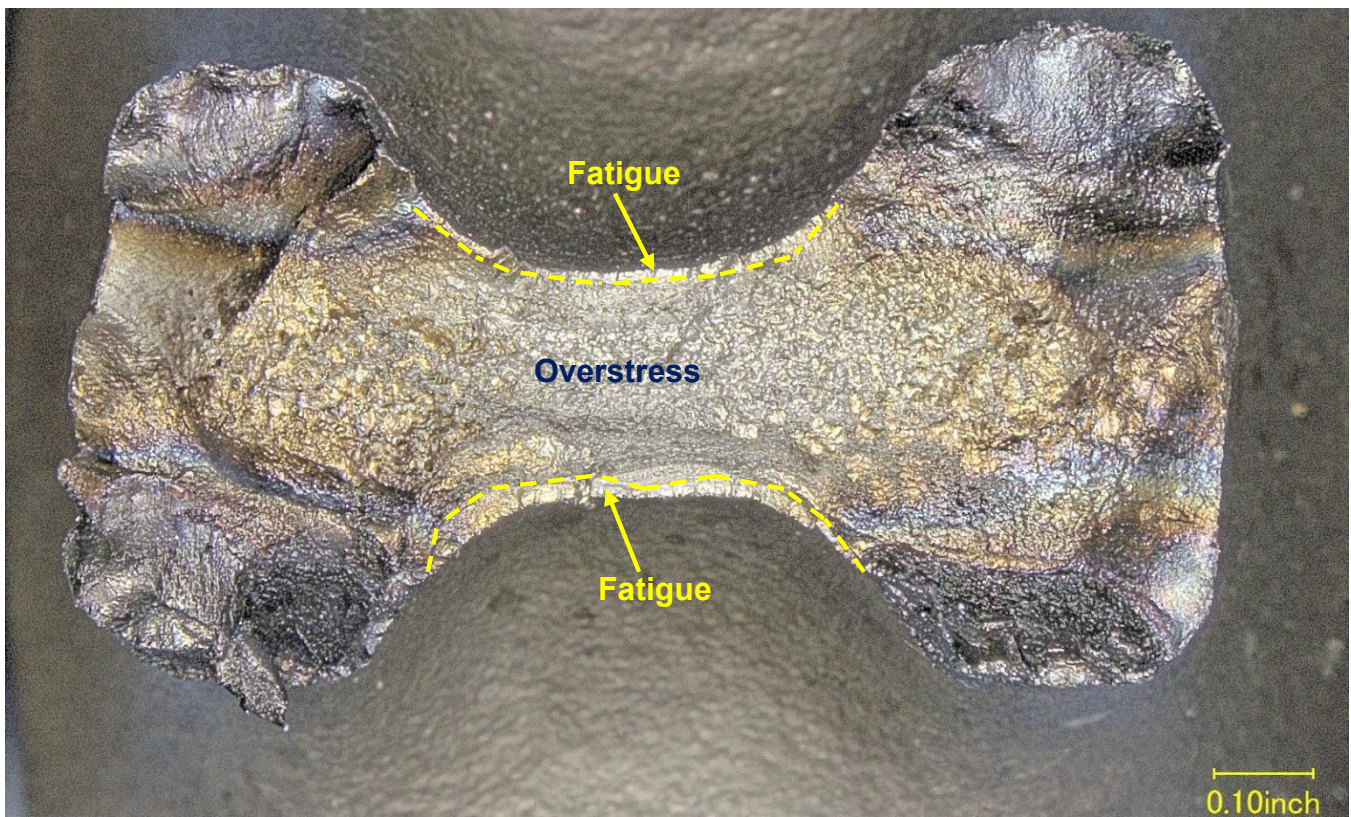


Figure 15 – The #2 connecting rod fracture surface, from the crankshaft side.

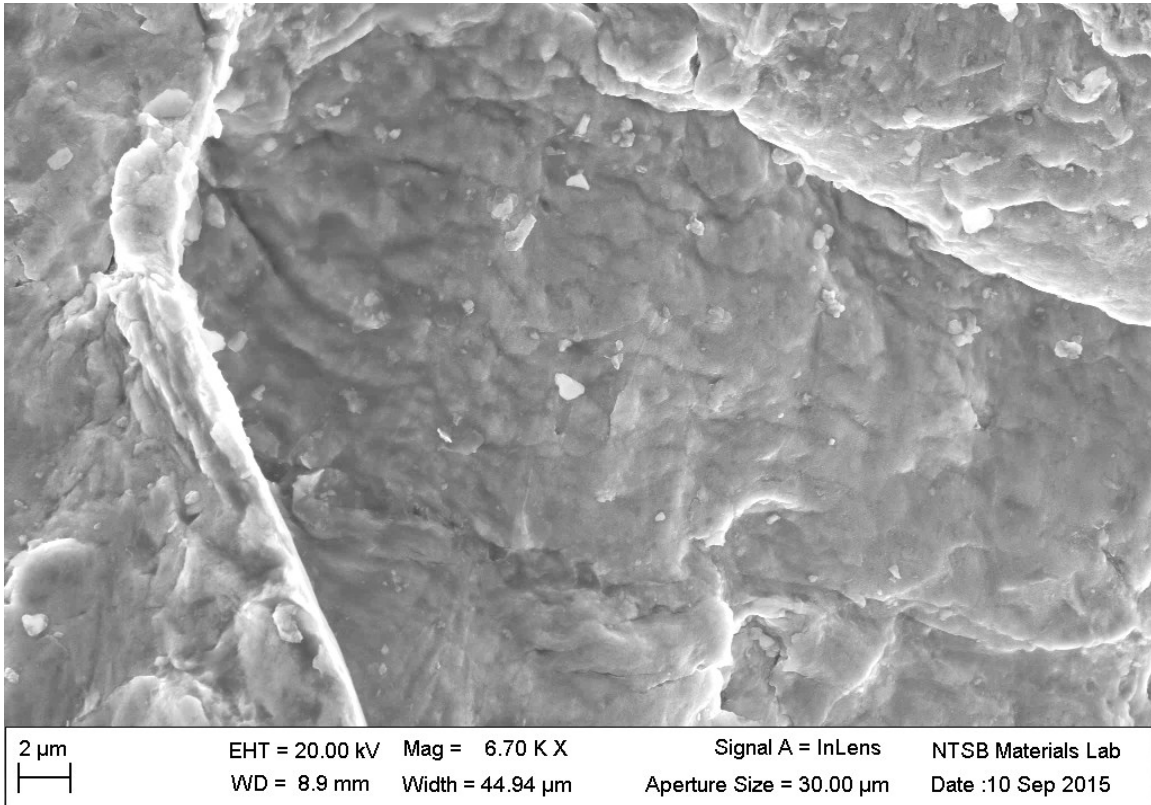


Figure 16 – SE micrograph of fatigue striations in the thumbnail crack portions of the #2 connecting rod fracture surface.

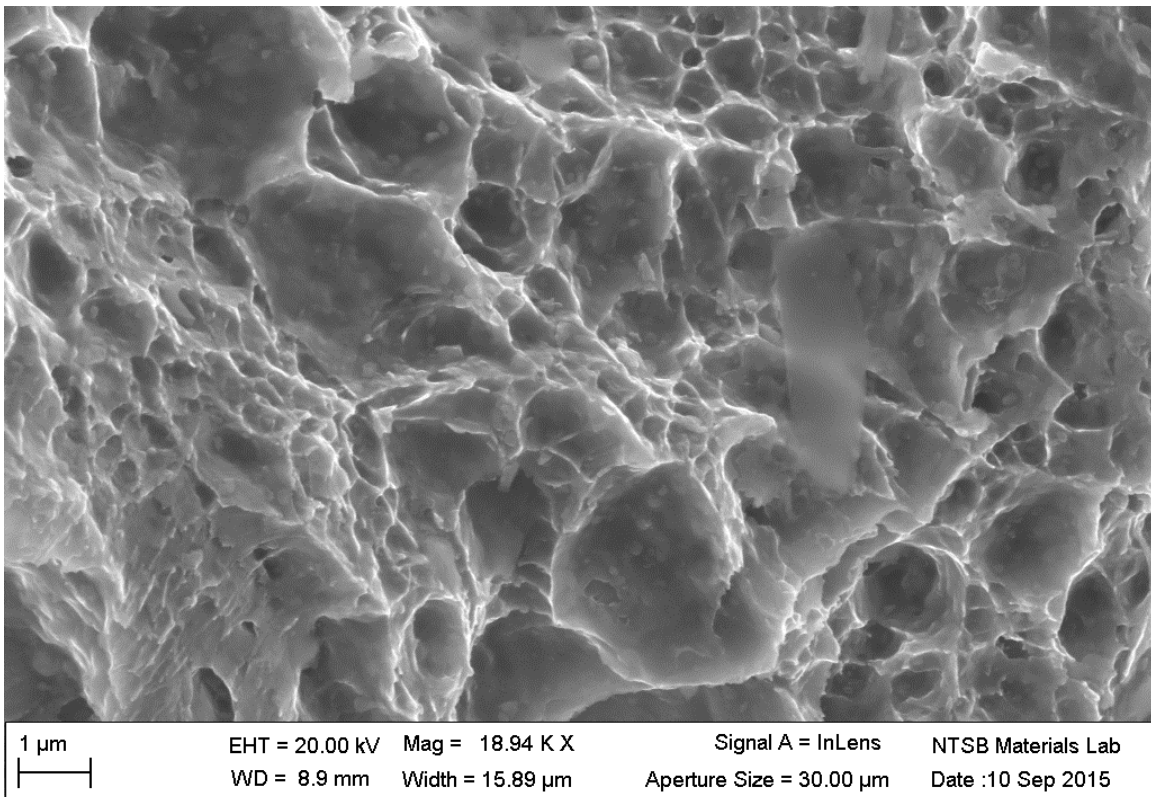


Figure 17 – SE micrograph of dimple rupture features present over most of the inner portions of the #2 connecting rod fracture surface.

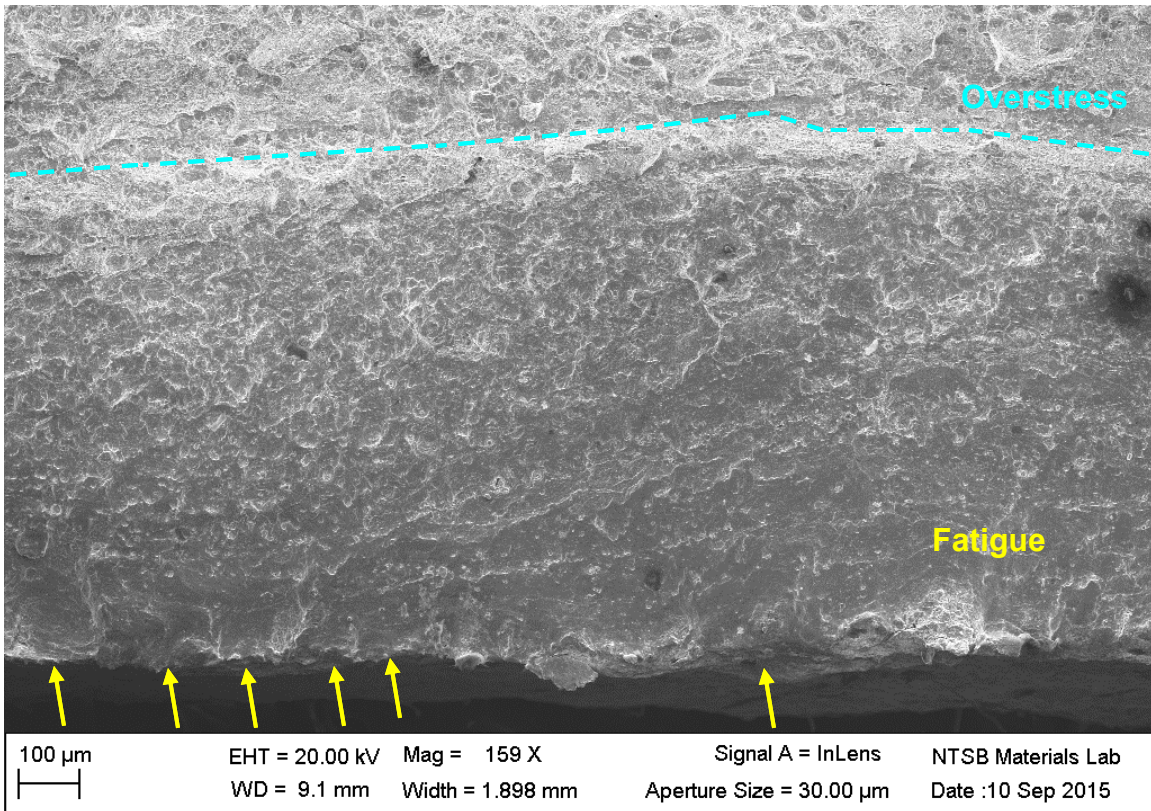


Figure 18 – SE micrograph of the fatigue region, showing multiple crack initiation sites (arrows) on the #2 rod surface.

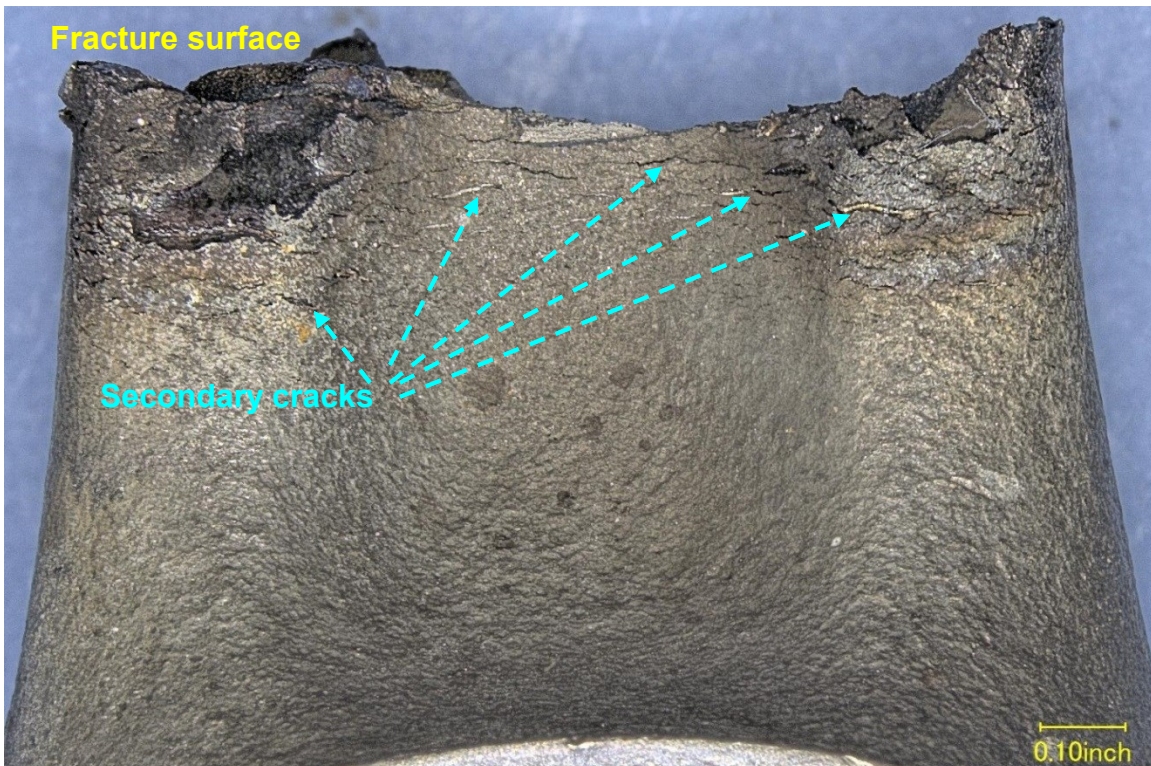


Figure 19 – The #2 connecting rod shaft near the fracture surface, from the side, showing secondary cracks below the fracture surface.

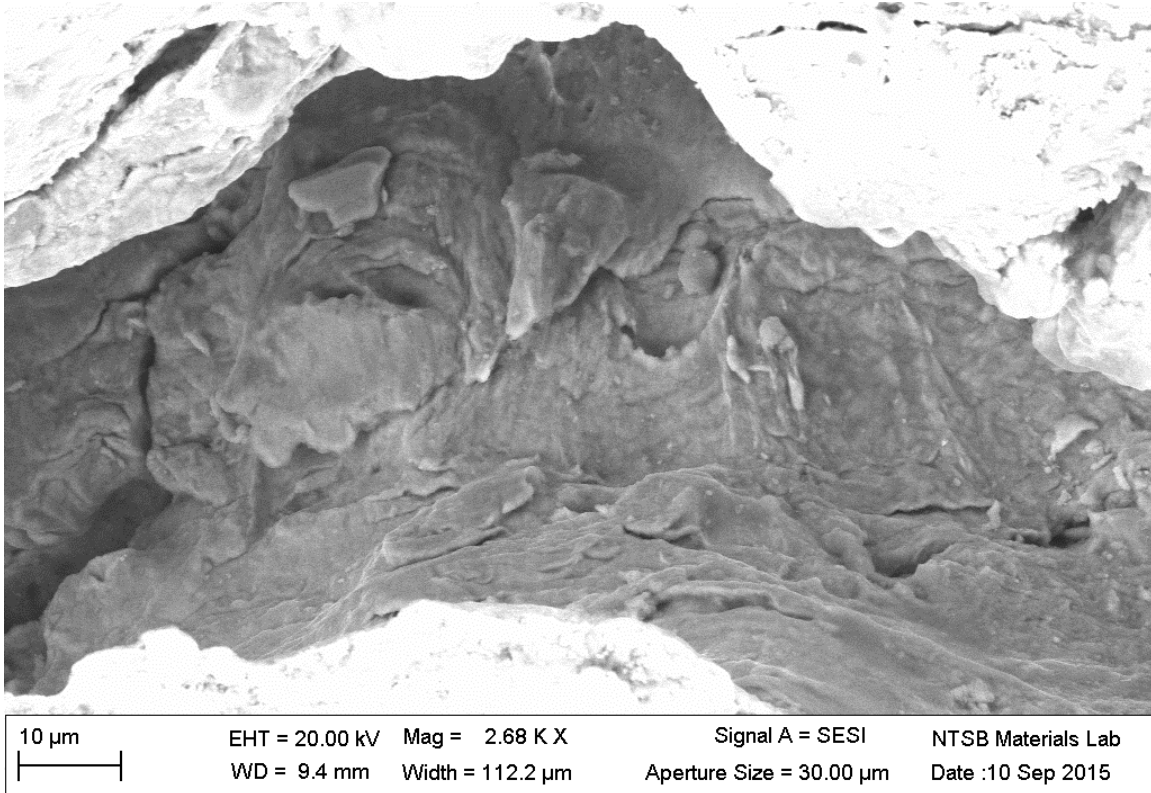


Figure 20 – SE micrograph of faint fatigue striations in the secondary cracks along the shaft of the #2 connecting rod (shown in Figure 19).



Figure 21 – Optical metallograph of a cross-section of the #2 connecting rod shaft, sectioned through two of the secondary cracks shown in Figure 19 and Figure 20 (etched 2% Nital).

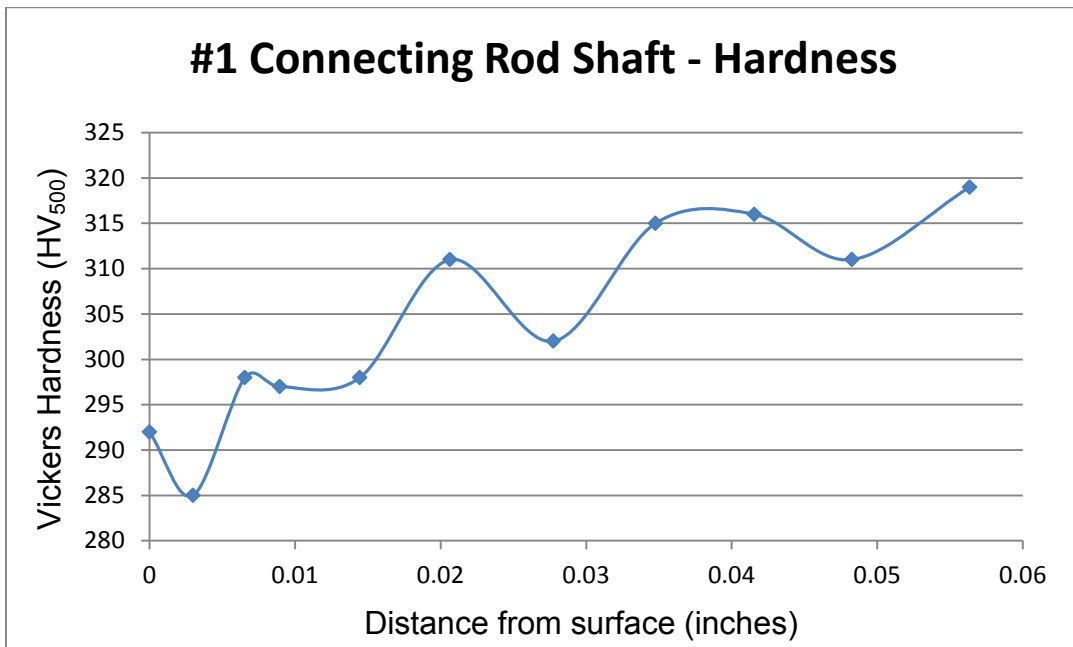


Figure 22 – Chart showing the hardness (HV₅₀₀) from the surface to the interior of connecting rod #1.

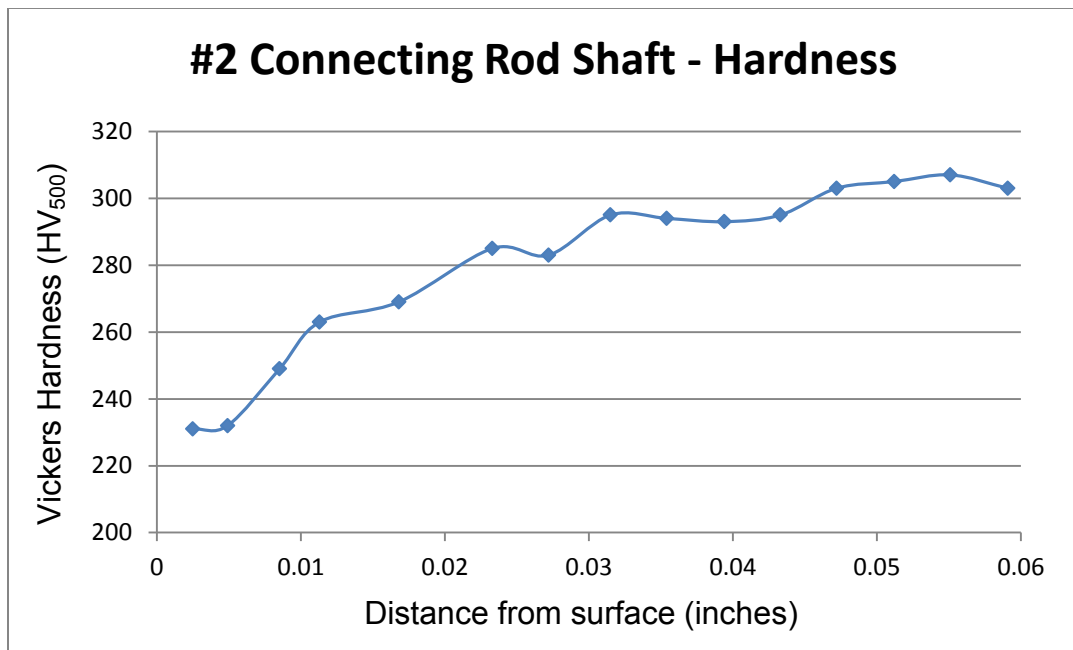


Figure 23 – Chart showing the hardness (HV₅₀₀) from the surface to the interior of connecting rod #2.